Available online at www.sciencedirect.com
SCIENCE DIRECT®
Journal of Crystal Growth 285 (2005) 24–30
JOURNAL OF CRYSTAL GROWTH
www.elsevier.com/locate/jcrysgro

Raman and photoluminescence studies on nanocrystalline ZnO grown on GaInPAs substrates

S.J. Chen[a,b], Y.C. Liu[c,*], H. Jiang[a], Y.M. Lu[a], J.Y. Zhang[a], D.Z. Shen[a], X.W. Fan[a]

[a]*Key Laboratory of Excited State Process, Changchun Institute of Optics, Fine Mechanics and Physics, Chinese Academy of Sciences, 16 East South Lake Avenue, Changchun 130021, People's Republic of China*
[b]*Graduate School of the Chinese Academy of Sciences, Beijing 100049, People's Republic of China*
[c]*Centre for Advanced Optoelectronic Functional Material Research, Northeast Normal University, Changchun 130024, People's Republic of China*

Received 5 June 2005; received in revised form 26 June 2005; accepted 14 July 2005
Available online 3 October 2005
Communicated by R. James

Abstract

Comprehensive Raman and photoluminescence (PL) results on ZnO nanocrystals are presented in this work. The ZnO nanocrystals were prepared by plasma-assisted electron beam evaporation of metallic Zn films on GaInPAs films, which were previously grown on InP substrates by MOCVD, then a low-temperature annealing process was conducted on the as-deposited Zn films. Raman results show the presence of a surface phonon (SP) mode, which reveals that nanocrystals are embedded in a compound matrix. Seven longitudinal optical-phonons (LOs) accompanied by SPs are observed in the resonant Raman spectrum for our ZnO nanocrystals at 80 K, which is probable due to a strong surface enhanced Raman scattering (SERS) effect and quantum confinement effect. Room temperature PL spectra show a single broad UV peak at around 3.45 eV with sharp Raman lines superimposed upon it, indicating a large quantum confinement effect in the ZnO nanocrystals due to their small dimensions. PL spectra measured at different temperatures show an anomalous dependence of the PL intensity with variation in temperature, which is analyzed on the basis of John-Singh's model. The total PL intensity is governed by the combination of radiative and non-radiative processes.

PACS: 63.22.+m; 78.55.−m; 61.82.Fk; 68.35.Ja

Keywords: A1. Photoluminescence; A1. Surface enhanced Raman scattering; A1. Surface phonon; B1. ZnO nanocrystals

*Corresponding author. Tel.: +86 431 5268803; fax: +86 431 5684009.
E-mail address: ycliu@nenu.edu.cn (Y.C. Liu).

0022-0248/$ - see front matter © 2005 Published by Elsevier B.V.
doi:10.1016/j.jcrysgro.2005.07.036

1. Introduction

Recently, the experimental and theoretical studies of semiconductor nanocrystallites [1–3] have generated tremendous technological and scientific interest, due to their unique electronic and optical properties and exhibition of new quantum phenomena. ZnO nanocrystals, especially, have been attracting much attention because of their large excitonic binding energy of about 60 meV, high mechanical and thermal stabilities, and the consequent potential application in opto-electronic devices.

The electronic, optical and vibrational properties of low-dimensional systems are sensitive not only to the dimensions but also to the shape and other growth-related complexities, such as the surface effects and size fluctuations. These properties contain information about many parameters, which are essential to the understanding of semiconductor device operation as well as the physics of the materials themselves. It is thus desirable to investigate in detail the change in electronic and vibrational properties of nanometer size structures with particular emphasis on the size and the growth conditions. Raman and PL are powerful non-destructive optical tools to study these changes.

In this paper, studies on ZnO nanocrystals were conducted by using Raman excited by the 488 nm line of an Ar^+ laser, resonant Raman scattering (RRS) excited by the 325 nm line of a He–Cd laser, room temperature PL, and temperature-dependent PL from 80 to 300 K.

2. Experimental procedure

The ZnO nanocrystals used in this study were prepared by plasma-assisted electronic beam evaporation of metallic Zn on GaInPAs films, following by a low-temperature annealing process in an oxygen atmosphere at different temperatures. GaInPAs films of 200 nm in thickness were previously grown on InP (1 0 0) substrates by metal organic chemical vapor deposition (MOCVD). GaInPAs films were used here as a buffer layer, in which phosphorus and arsenic anions diffused into Zn films easily and chemically combined with Zn, acted as a shell layer capping the ZnO nanocrystals. Subsequently, tens of nanometers of Zn films were deposited on GaInPAs films by an electronic beam evaporation method assisted with an oxygen plasma. In this experiment, an oxygen plasma was introduced into the reactor chamber during Zn evaporation (duration: 30 min). The chamber pressure was held at 2.0×10^{-2} Pa, the energy of the plasma used was 100 eV, and the voltage of the accelerator was 100 V. The thickness of the as-deposited Zn film is about 60 nm in order to get nano-sized crystalline ZnO films. Subsequently, the film was divided into four parts. Three parts were separately annealed in a thermal tube furnace in an oxygen ambient at 300, 400 and 500 °C for 1 h, respectively.

Raman experiments were performed using a HR 800 JY laser Raman spectrometer. The Raman spectra were recorded in a back scattering geometry using the 488 nm line of an argon ion laser. PL and resonant Raman measurements were made using the same setup as used for Raman except using a 325 nm He–Cd laser as the excitation light. The temperature-dependent PL studies were carried out using a closed cycle refrigeration system at temperatures ranging from 80 to 300 K.

3. Results and discussion

The wurtzite structure ZnO belongs to the space group C_{6v}^4 with two formula units per primitive cell, and all atoms occupying C_{3v} sites. Zone center optical phonons predicted by group theory are $A_1 + 2E_2 + E_1$. Of these the phonons of A_1 and E_1 symmetry are polar and hence exhibit different frequencies for the transverse-optical (TO) and longitudinal-optical (LO) phonons. For this system anisotropy splitting is found to be much smaller than the LO–TO splitting. This is evident from the reported single-crystal Raman spectrum [4].

Fig. 1 shows the Raman spectra of a ZnO nanocrystal sample excited by a 488 nm line of an Ar^+ laser. The Raman spectrum of the as-deposited sample shows a broad hump at

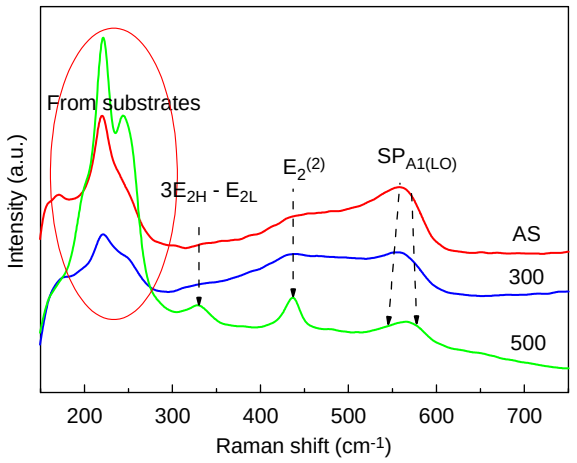

Fig. 1. Raman spectra of ZnO nanocrystal samples.

560 cm^{-1} with a big shoulder at its lower frequency side in addition to weak features at 437 and 330 cm^{-1}. Besides, several prominent peaks were observed at frequencies below 300 cm^{-1}. As for the broad hump at 560 cm^{-1}, the Raman spectrum of the sample annealed at 300 °C for an hour shows an up-shift of 4 cm^{-1} from the peak position and decreases in intensity from the as-deposited sample. It is found that with increasing annealing temperature, the Raman spectrum shifts towards higher frequency, becomes narrower and is less asymmetric. The Raman spectrum of the sample annealed at 500 °C exhibits three obvious peaks at 330, 437 and 575 cm^{-1}, respectively, in addition to several strong peaks at low frequencies below 300 cm^{-1}.

Based on the reported zone-center optical phonon frequencies in ZnO [4], the Raman peak at 437 cm^{-1} should be assigned to the E_{2H} mode; the peak at 330 cm^{-1} should be assigned to the second-order Raman spectrum arising from zone-boundary phonons $3E_{2H}$–E_{2L}; the hump at 575 cm^{-1}, which evolved from the broad hump at 560 cm^{-1} for the as-deposited sample with increasing annealing temperature, can be described by two superimposed peaks. The peak locates at 580 cm^{-1}, can be assigned to A_{1LO} modes. Another one locates at around 560 cm^{-1} (between the bulk TO and LO phonon peaks) decreases in intensity and shifts to lower frequency as the annealing temperature increases. According to electromagnetic theory [5] (Ruppin and Englman 1970, Ruppin 1982), the surface phonon (SP) peak shows the following three characteristic features: (i) the peak is located between the bulk TO and LO peaks; (ii) the peak shifts to lower frequency as ε_m increases; and (iii) the intensity of the peak decreases as the particle size increases. The behavior of the new peak seen in Fig. 1 corresponds well to the above characteristic features of the SP peak. With increasing annealing temperature, ZnO nanocrystals are expected to grow gradually, which results in a decrease of the metallic Zn at the surface layer, and ε_m is expected to increase when the Zn-rich outer layer is continuously oxidized. Basing on the aforementioned argument, the new peak is assigned to the SP mode. Presence of the SP mode gives evidence that ZnO nanocrystals were obtained and imbedded in the matrix. The strong peaks at the lower frequency side below 300 cm^{-1} in the Raman spectra should be assigned to the GaInPAs substrate and its oxides.

Resonant Raman scattering from solids can be observed if the energy of the incoming or scattered photons matches real electronic states in the material. This behavior results when the denominator in the Raman scattering cross-section term is close to zero. In resonant Raman scattering, where the exciting photon energy is resonant with the electronic interband transition energy, the polar symmetry A_1 and E_1 modes are dominant. Longitudinal optical phonons are known to exhibit stronger resonance enhancement than other modes. Multiphonon scattering processes were previously reported for single crystalline bulk ZnO [6], and recently for ZnO films [7], ZnO nanowires [8] and high conductive ZnO layers [9]. The resonant Raman spectrum was also measured for our ZnO nanocrystalline sample at low temperature (80 K) using a 325-nm He–Cd laser as the excitation source. The spectrum from the as-deposited sample, as shown in Fig. 2, consists of a broad luminescence envelope peaking at about 356 nm, with relatively sharp lines superimposed upon it. These sharp lines are at frequency shifts which are multiples of the 1-LO zone-center frequency of 580 cm^{-1}. Note that 7 LO were

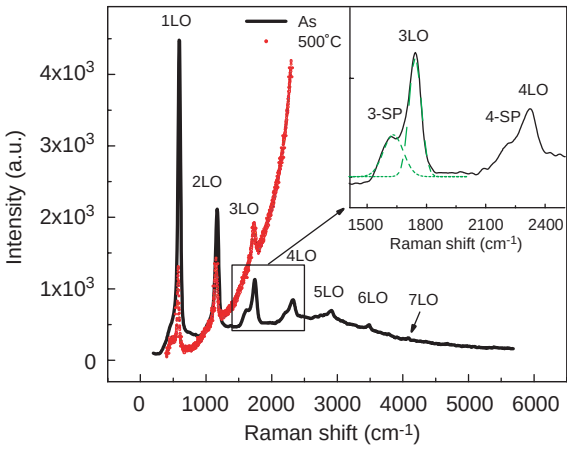

Fig. 2. Resonant Raman spectra of the as-deposited sample and the sample annealed at 500 °C.

observed in our ZnO nanocrystals. The result could be comparable with that from single crystalline bulk ZnO [6], and it is much better than that from ZnO films [7] and nanowires [8]. Only 3 weak LO phonon energy shifts were observed from the sample annealed at 500 °C, as shown in Fig. 2.

Two factors are considered to explain the much enhanced resonant Raman scattering signals from our ZnO nanocrystals. One is a surface enhanced Raman scattering (SERS) effect [10] due to metal Zn ions on the surface layer of the ZnO nanocrystals. The SERS effect exploits a property of nanometer-sized metal particles or surface grains. Incident laser photons are absorbed into the metal particles through oscillations of the surface electron charge density (plasmons). This can couple with molecules in proximity and provide an efficient pathway to transfer energy to the molecular vibrational modes, and generate Raman photons. The enhancement is maximized when the metal grains are smaller than the incident laser wavelength, and the metal has the optical properties required to generate surface plasmons. This argument is supported by the result that the sample annealed at 500 °C shows a smaller number of observable multiphonon (3LO) and weak signals in the resonant Raman spectra, as shown in Fig. 2, since no metal Zn ions remained on the surface of ZnO nanocrystals after annealing at higher temperature. A second factor is quantum confinement effects, which enlarge the band gap of nanometer-sized ZnO crystals. The E_1 energy gap of our ZnO nanocrystals is estimated to be 3.51 eV, according to our measured PL UV peak energy of 3.46 eV and adding an exciton binding energy of 60 meV. This value is closer to the energy of the laser photons (3.81 eV) compared to the energy gap of bulk ZnO (3.37 eV). The scattering cross section would enhance as the E_1 energy gap moves closer to the energy of the laser photons, which results in a much enhanced Raman scattering intensity.

There is a shoulder on the lower frequency side of every LO phonon. It is weakly observed at 1 LO, but the intensity of the shoulder is enhanced with increasing number of the multiphonon and distinguishes itself at 3 LO and 4 LO, which is shown in the inset of Fig. 2. Judging from its third-order peak of multiphonon at 1632 cm^{-1}, which is far from that of 3 LO at 1743 cm^{-1}, this new peak cannot be attributed to $E_{1\text{-LO}}$–$A_{1\text{-LO}}$ splitting, since this splitting should fit the formula $\lambda(n\text{LO}) = 9n = 27\,cm^{-1}$ [11]. Its first-order peak located at $1662/3 = 554\,cm^{-1}$, is almost at the same position as the SP peak obtained from the above Raman results. So this peak should be assigned to the SP peak, consistent with the previously described Raman results. The observation of SP mode and its multiphonons under resonant excitation condition has never been reported, which gives further evidence that ZnO nanocrystals are imbedded in the matrix.

Fig. 3 shows the room-temperature PL results from the as-deposited sample and the samples annealed at different temperatures. The room temperature PL spectrum from the as-deposited sample is observed as a single broad peak in the UV region with relatively sharp Raman lines superimposed upon it. This UV emission peak is observed at around 3.45 eV, having a big shift from that of bulk ZnO (3.37 eV). Its peak positions shift monotonically to lower energies with increasing of the annealing temperature. PL from the sample annealed at 500 °C is found to show a very strong narrow UV peak at 3.28 eV and a weak broad peak at around 2.4 eV. The UV emission is attributed to the near-band-edge (NBE) emission,

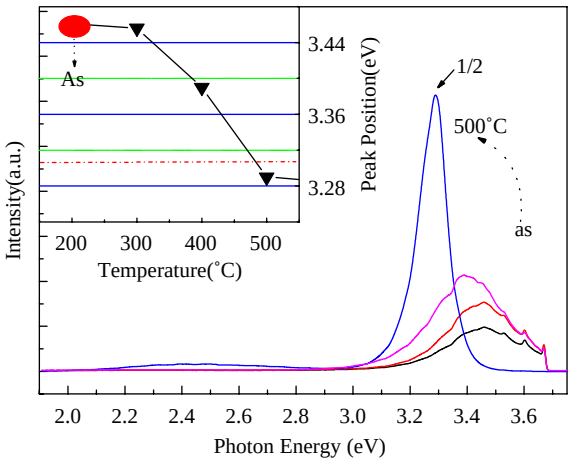

Fig. 3. Room-temperature PL of the as-deposited sample and the samples annealed at different temperatures.

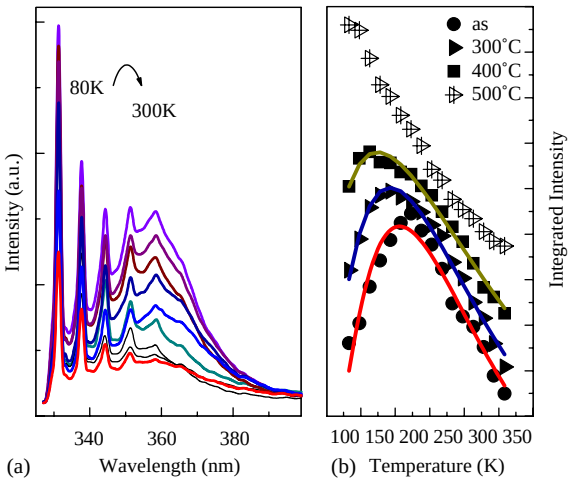

Fig. 4. (a) PL spectra from the as-deposited sample measured at different temperatures ranging from 80 to 300 K. (b) Theoretical fits to the experimental points of the integrated intensity vs. temperature.

and the visible emission is attributed to deep-level (DL) emission, respectively.

Quantum confinement effects have been proposed by various authors [12–16] to explain the room temperature PL. In this model, quantum confinement effects enlarge the band gap of nanometer size clusters, increase the oscillator strength, and give rise to efficient and UV luminescence. The UV peak of the PL spectra from our ZnO nanocrystals shows a large blue shift from that of bulk ZnO due to strong quantum confinement effects, which indicates that nanometer size ZnO clusters were obtained. The size of the cluster can be calculated by using the expression for the energy gap, including the quantum confinement effect [17]:

$$E_g \approx E_{g0} + \frac{h^2\pi^2}{2d^2\mu} - \frac{1.8e^2}{\varepsilon d}, \quad (1)$$

where E_{g0} is the energy gap for bulk materials, d is the particle size, $(1/\mu) = (1/m_e) + (1/m_h)$ (m_e and m_h are the electron and hole effective masses, respectively), and ε is the dielectric constant, For ZnO, the effective masses of electrons and holes are $0.38m_0$ and $1.80m_0$, respectively, and the dielectric constant is 8.75 [18]. Thus we infer that the mean grain sizes of our ZnO nanocrystals are 12.1, 12.8, 14.2, and 46 nm for the as-deposited sample and the samples annealed at 300, 400 and 500 °C, respectively.

Fig. 4 (a) shows the PL spectra from the as-deposited sample measured at different temperatures ranging from 80 to 300 K. The PL lineshape does not seem to change much with temperature variation. The variation of PL intensity is given in Fig. 4(b). It is noted that the PL intensity shows anomalous dependence with variation in temperature. A similar temperature behavior is frequently reported for semiconductor quantum dots [19,20]. The above results are analyzed on the basis of John-Singh's model [21]. According to this model, the temperature dependence of luminescence can be analyzed in terms of competition between the radiative and the non-radiative hopping processes. The radiative process shows a temperature dependence of the Arrhenius type [22]:

$$R_r = v_r \exp\left(\frac{T_r}{T}\right), \quad (2)$$

where T_r is a characteristic activation temperature pertaining to the radiative recombination, and v_r is the characteristic frequency. The escape rate is hypothesized to have a Berthlot-type dependence [23,24]. Accordingly, R_{hop} can be written as

$$R_{hop} = v_B \exp\left(\frac{T}{T_B}\right), \quad (3)$$

where T_B is the characteristic Berthlot temperature associated with the escape process, and ν_B is the characteristic frequency. The PL intensity at temperature T can be given by

$$I(T) = \frac{I_0}{1 + \nu_0 \exp((T/T_B) + (T_r/T))}, \quad (4)$$

where $\nu_0 = \nu_B/\nu_r$ is the reduced frequency.

Fig. 4(b) shows the theoretical fits to the experimental points of the integrated intensity vs. temperature using Eq. (4). The agreement between the theory and the experiment is found to be excellent. The characteristic Berthlot temperature T_B and the radiative temperature T_r are calculated from these fits. The equation implies a maximum of the PL intensity at temperature $T_m = \sqrt{T_r T_B}$. The values of T_B, T_r and T_m as a function of annealing temperature are tabulated in Table 1.

For annealing temperatures up to 400 °C, the Berthlot temperature increases from 111 to 206 K, and the radiative temperature decreases from 220 to 75 K. It is found that the temperature T_m corresponding to the maxima is largest for the as-deposited sample and smallest for the sample annealed at 400 °C. The radiative temperature T_r indicates the activation energy, and for our samples the activation energy lies in the range of 6.5–17.85 meV. The activation energy can take a range of values due to inherent disorder in these materials. It is found that the activation energy decreases for increasing annealing temperature.

As for the sample annealed at 500 °C, the PL intensity monotonously decreases with an increase of temperature in the range of 80–300 K, which is similar to the temperature-dependent behavior of ZnO films [25,26].

The decrease of PL intensity at lower temperature could be due to tunneling of carriers from the crystallites to non-radiative centers [27]. This is possible due to long radiative life-times at low temperatures. The maximum in the PL intensity vs. temperature occurs at a specific temperature, which is dependent on the crystallite size. At this temperature the radiative transitions, owing to the small activation energy, are fast enough to overwhelm the tunneling process, and the thermally activated escape processes are still not important due to the relatively large activation energy for the non-radiative processes. The total PL intensity is governed by the combination of radiative and non-radiative processes.

Table 1
The values of T_B, T_r and T_m as a function of annealing temperature

	As-deposited	300 (°C)	400 (°C)	500 (°C)
T_B(K)	111	143	206	
T_r	220	141	75	
T_m	156	142	124	

4. Conclusion

ZnO nanocrystals were prepared on GaInPAs/InP substrates by a simple method of plasma-assisted electron-beam evaporation of metallic Zn films, following by a low-temperature annealing process. Raman results reveal the nanocrystals are embedded in a compound matrix, in which a SP mode was detected. Resonant Raman spectrum shows 7 LO accompanied by SPs in our ZnO nanocrystals at 80 K. The SERS and quantum confinement effects are considered to explain this phenomenon. Room temperature PL spectra show a single broad UV peak at around 3.45 eV with sharp Raman lines superimposed upon it, indicating a large quantum confinement effect in the ZnO nanocrystals due to their small dimensions. John-Singh's model was used to analyze the anomalous dependence of the PL intensity with variation in temperature. The total PL intensity is governed by the combination of radiative and non-radiative processes.

Acknowledgements

This work is supported by the National Natural Science Foundation of China Nos. 60376009, 60278031, the Major Project of the National Natural Science Foundation of China No. 60336020 and the Cultivation Fund of the Key Scientific and Technical Innovation Project, Ministry of Education of China (No. 704017), Science

Foundation for Yong Teachers of Northeast Normal University (20050202).

References

[1] F. Henneberger, S. Schmitt-Rink, E.O. Gabel, Optics of Semiconductor Nanostructures, Academic Verlag, Berlin, 1993.
[2] M. Read, W. Kirk (Eds.), Nanostructures and Mesoscopic Systems, Academic Verlag, San Diego, 1991.
[3] P. Mishra, K.P. Jain, Phys. Rev. B 62 (2000) 14790.
[4] C.A. Arguello, D.L. Rousseau, S.P.S. Porto, Phys. Rev. 181 (1969) 1351.
[5] R. Ruppin, J. Phys. C: Solid State Phys. 8 (1975) 1969; R. Ruppin, R. Englam, in: G.B. Wright (Ed.), Light Scattering Spectra of Solids, Springer, New York, 1969, pp. 157–166.
[6] J.F. Scott, Phys. Rev. B 2 (1970) 1209.
[7] X.T. Zhang, Y.C. Liu, Z.Z. Zhi, J.Y. Zhang, Y.M. Lu, D.Z. Shen, W. Xu, G.Z. Zhong, X.W. Fan, X.G. Kong, J. Phys. D 34 (2001) 3430.
[8] H.T. Ng, B. Chen, J. Li, J. Han, M. Meyyappan, J. Wu, S.X. Li, E.E. Haller, Appl. Phys. Lett. 82 (2003) 2023.
[9] V.V. Zalamai, V.V. Ursaki, E.V. Rusu, P. Arabadji, I.M. Tiginyanua, L. Sirbu, Appl. Phys. Lett. 84 (2004) 5168.
[10] M. Moskovits, Rev. Mod. Phys. 57 (1985) 783.
[11] J.F. Scott, Phys. Rev. B 2 (1970) 1209.
[12] L.T. Canham, Appl. Phys. Lett. 57 (1990) 1046.
[13] A.J. Read, R.J. Needs, K.J. Nash, L.T. Canham, P.D.J. Calcott, A. Qteish, Phys. Rev. Lett. 69 (1992) 1232.
[14] A.G. Cullis, L.T. Canham, Nature 353 (1991) 335.
[15] G.D. Sanders, Y.-C. Chang, Appl. Phys. Lett. 60 (1992) 2525.
[16] T. Takagahara, K. Takeda, Phys. Rev. B 46 (1992) 15578.
[17] S. Cho, J. Ma, Y. Kim, Y. Sun, G.K.L. Womg, Appl. Phys. Lett. 75 (1999) 2761.
[18] L.E. Brus, J. Chem. Phys. 80 (1984) 4403.
[19] D.I. Lubyshev, P.P. Gonzales-Borrero, E. Bowers, E. Marega Jr., E. Petitprez, N. LaScalla Jr., P. Basmaji, Appl. Phys. Lett. 68 (1996) 205.
[20] G. Wang, S. Fafard, D. Leonard, J.L. Merz., P.M. Petroff, Appl. Phys. Lett. 64 (1994) 2815.
[21] G.C. John, V.A. Singh, Phys. Rev. B 54 (1996) 4416.
[22] Y. Kanemitsu, Phys. Rev. B 53 (1996) 13515.
[23] H. Berthlot, Ann. Chem. Phys. 66 (1962) 110.
[24] C.M. Hurd, J. Phys. C 18 (1985) 6487.
[25] S.J. Chen, Y.C. Liu, J.Y. Zhang, Y.M. Lu, D.Z. Shen, X.W. Fan, J. Phys.: Condens. Matter 15 (2003) 1975.
[26] S.J. Chen, Y.C. Liu, J.G. Ma, D.X. Zhao, Z.Z. Zhi, Y.M. Lu, J.Y. Zhang, D.Z. Shen, X.W. Fan, J. Crystal Growth 240 (2002) 467.
[27] J.C. Vial, A. Bsiesy, F. Gaspard, R. Herino, M. Ligeon, F. Muller, R. Romestain, R.M. Macfarlane, Phys. Rev. B 45 (1992) 14171.